Fusion excitation functions and barrier distributions: A semiclassical approach

Giovanni Pollarolo

Dipartimento di Fisica Teorica, Universitá di Torino, and Istituto Nazionale di Fisica Nucleare, Sezione di Torino, Via Pietro Giuria 1, I-10125 Torino, Italy

Aage Winther

The Niels Bohr Institute, Blegdamsvej 17, DK-2100 Copenhagen Ø, Denmark

Fusion cross sections and barrier distributions are discussed and calculated in the framework of a semiclassical approximation for a variety of systems. An overall good description of the data is achieved.

I. INTRODUCTION

In a collision between two ions the process that brings them to form a single composite system is called fusion. The simplest description of this process considers the two ions as rigid spherical objects that interact via a repulsive, Coulomb, plus an attractive, nuclear, potentials depending only on the relative center-of-mass distance. Fusion is, in this model, described as the ability of the system to penetrate the potential energy barrier. A systematic study of fusion data with this model can be found in Ref. [1].

However, many experiments have shown that the barrier penetration model is inadequate for the description of the observed cross sections, at energies below the Coulomb barrier the model underpredicts, of several orders of magnitude, the observed values [2]. These discrepancies have been readily attributed to the effect of coupling of the relative motion to the internal degrees of freedom of the two colliding ions. The factors that have been identified as playing a major role in the enhancement of the sub-barrier fusion are permanent nuclear deformation, coupling to the low-lying nuclear excited states, and, possibly, particle transfer (in particular neutrons). In a simple approximation, where one neglects the excitation energy of the reaction channels, one can interpret the effect of the couplings as giving rise to a distribution of barriers which drastically alters the fusion probability from its value calculated with a single barrier [3].

Following this idea a method was proposed [4] for extracting the barrier distribution from accurate measurements of the fusion excitation function $\sigma(E)$ by taking the second derivative with respect to the center-of-mass energy (E) of the quantity $E\sigma(E)$. While the fusion excitation function is almost featureless, the barrier distributions display a very sensitive pattern as a function of the different colliding partners so that the effects of the couplings are shown explicitly.

From a theoretical point of view, the standard way to address the influence of the coupling between the relative motion and the intrinsic degrees of freedom is through the use of the coupled-channels formalism. This implies that very large numerical calculations should be done in order to describe the low-energy fusion data. These calculations, over the years, have been done with several degrees of sophistication including couplings to static deformation, to vibrational states and, to some degree, also to transfer channels

[5–10]. All these calculations have been able to describe quite well the excitation function while they had several problems in the description of the barrier distributions.

In this contribution we will describe fusion excitation functions and barrier distributions using the semiclassical model developed in Refs. [11,12] where the coupling to the low-lying surface modes and the transfer of nucleons (neutrons and protons) are taken explicitly into account in a semiclassical approximation. The same model has been successfully applied to the study of multinucleon transfer reactions and to the description of the transition between the quasielastic reactions and the more complicated deep-inelastic collisions. The paper after a detailed summary of the theoretical concepts (Sec. II) applies the obtained results to calculate fusion excitation functions and barrier distributions for several combinations of targets and projectiles (Sec. III).

II. THE THEORY

From the study of heavy-ion reactions we have learned that the transition from the grazing regime to the more complicated deep-inelastic regime may be described quite well in the semiclassical approximation in term of the well known form factors for single-nucleon transfer and the excitation of the low-lying surface vibrations. In term of these building blocks the Hamiltonian is written in the form

$$\hat{H} = \hat{H}_a + \hat{H}_A + \hat{V}_{int}(t), \tag{1}$$

where for the projectile (a) we can write

$$\hat{H}_a = \sum_i \epsilon_i a_i^\dagger a_i + \sum_{\lambda\mu} \hbar\omega_\lambda a_{\lambda\mu}^\dagger a_{\lambda\mu}. \tag{2}$$

The first sum defines the single particle Hamiltonian, the operators $a^\dagger(a)$ are the fermion operators that create (annihilate) a particle on the single-particle level with energy ϵ_i and quantum number $i \equiv (nljm)$, while the second sum defines the Hamiltonian for the excitation of the surface mode, $a_{\lambda\mu}^\dagger(a_{\lambda\mu})$ are the boson operators for the creation (annihilation) of a phonon of multipolarity $\lambda\mu$ and energy $\hbar\omega_\lambda$. A similar expression holds for the Hamiltonian of the target system (A).

The interaction $\hat{V}_{int}(t)$ has three terms

$$\hat{V}_{\text{int}}(t) = \hat{V}_{tr}(t) + \hat{V}_{in}(t) + \Delta U_{aA}(t). \qquad (3)$$

The first, responsible for transfer, is written in the form

$$\hat{V}_{tr} = \sum_{(\nu\pi)j,k} f^{a_k a'_j}(\mathbf{r}(t)) a^\dagger(a_k) a(a'_j)$$

$$+ \sum_{(\nu\pi)j,k} f^{a'_k a_j}(\mathbf{r}(t)) a^\dagger(a'_k) a(a_j), \qquad (4)$$

where $f^{a_k a'_j}$ and $f^{a'_k a_j}$ are the single particle stripping and pick-up form factors. The sum has to be extended over all single particle levels (a_k, a'_j) of neutrons (ν) and protons (π) of target and projectile. For the inelastic processes (excitation of surface vibrations) we write

$$\hat{V}_{in} = \sum_{\lambda\mu} f^A_{\lambda\mu}(\mathbf{r}) [a^\dagger_{\lambda\mu}(A) + a_{\lambda\mu}(A)]$$

$$+ \sum_{\lambda\mu} f^a_{\lambda\mu}(\mathbf{r}) [a^\dagger_{\lambda\mu}(a) + a_{\lambda\mu}(a)], \qquad (5)$$

where $f^A_{\lambda\mu}$ and $f^a_{\lambda\mu}$ are the nuclear plus Coulomb form factors for the excitation of the surface modes in the target and in the projectile. The last term of the interaction ΔU_{aA} takes into account the modification of the effective potential for the radial motion. The most important modifications are due to proton transfer, that alters the Coulomb potential, and the transfer of angular momentum due to the surface vibrations, that alters the centrifugal term (see below).

The time dependence of the interaction is obtained, in the semiclassical approximation, by solving the classical equation of motion in a nuclear plus Coulomb field. For the nuclear potential U_{aA} we use the simple parametrization [13]

$$U_{aA} = -16\pi\gamma a \frac{R_a R_A}{R_a + R_A} \frac{1}{1 + \exp[(r - R_a - R_A)/a]} \qquad (6)$$

whose parameters come from the knowledge of the nuclear densities and have been slightly adjusted through a systematic comparison of elastic scattering data. They are given by

$$\frac{1}{a} = 1.17[1 + 0.53(A_a^{-1/3} + A_A^{-1/3})] \text{ fm}^{-1}, \qquad (7)$$

$$R_i = 1.2 A_i^{1/3} - 0.09 \text{ fm}, \qquad (8)$$

$$\gamma = 0.95 \left(1 - 1.8 \frac{(N_a - Z_a)(N_A - Z_A)}{A_a A_A}\right) \text{ MeV fm}^{-2}, \qquad (9)$$

where A_i, Z_i, and N_i are the mass, charge, and neutron numbers of nucleus i. The Coulomb potential is taken to be of the usual point charge form.

Neglecting the coupling terms, at a given center-of-mass energy E, the fusion cross section is written as

$$\sigma(E) = \sum_l \frac{\pi\hbar^2}{2m_{aA}E} (2l+1) T_l(E), \qquad (10)$$

where $T_l(E)$ is the transmission probability through the potential barrier of partial wave l. At energies above the Coulomb barrier it is convenient to rewrite Eq. (10) in the sharp cutoff model where one assumes that $T_l = 1$ for all partial waves leading to a distance of closest approach smaller than a certain value r_c beyond which the two ions fuse. In this approximation one obtains

$$\sigma(E) = \pi r_c^2 \left(1 - \frac{U_{aA}(r_c)}{E}\right). \qquad (11)$$

At energies close to or below the Coulomb barrier, the above approximation has to be modified by including the penetration probability through the barrier. Using the inverse parabolic approximation the transmission coefficient becomes

$$T_l(E) = \frac{1}{1 + \exp[2\pi(E_b - E)/\hbar\omega_b]}, \qquad (12)$$

where E_b is the barrier of the effective potential and ω_b the frequency in the relative motion

$$\omega_b = \sqrt{\frac{1}{m_{aA}} \frac{\partial^2 U_{\text{eff}}}{\partial r^2}}. \qquad (13)$$

The fusion cross section calculated with this transmission coefficient constitutes the no-coupling limit and, as mentioned in the Introduction, underestimates considerably the actual fusion cross section data.

For the capture distance r_c one usually uses the Coulomb barrier radius r_B, but simple classical calculations demonstrate (see Refs. [14,15]) that at short distances the reaction is strongly influenced by considering the deformation degrees of freedom α. These surface degrees of freedom may indeed give rise to instabilities (i.e., capture) for trajectories well outside the Coulomb barrier, i.e., for trajectories with an l value greater than the l grazing. In order to give an estimation of the capture angular momentum l_c and the capture distance r_c we have to study the problem of the merging of the two nuclear surfaces, in other words we must know if at the turning point the surface distance $s = r - R_a - R_A$ will increase or decrease. From the classical equations of motion, at the turning point we can write

$$m_{aA}\ddot{s} = \frac{l^2}{m_{aA}r^3} + \frac{Z_a Z_A e^2}{r^2} - (1+\delta)\frac{\partial U_{aA}}{\partial r} \qquad (14)$$

with

$$\delta = \sum_{\lambda_n} \frac{2\lambda_n + 1}{4\pi} \left[(R_a^0)^2 \frac{m_{aA}}{D_\lambda^a(n)} + (R_A^0)^2 \frac{m_{aA}}{D_\lambda^A(n)}\right], \qquad (15)$$

$D_\lambda^i(n)$ being the mass parameters of the surface modes of target and projectile.

If $\ddot{s} < 0$, large deformation will occur and the system will merge to form a compound. The boundary of grazing reactions may thus be calculated from the condition that $\ddot{s} = 0$. This leads to the equations

$$\frac{l_c^2}{m_{aA}r_c^3}+\frac{Z_aZ_Ae^2}{r_c^2}-(1+\delta)\frac{\partial U_{aA}}{\partial r}\Bigg|_{r_c}=0, \qquad (16)$$

$$\frac{l_c^2}{2m_{aA}r_c^2}+\frac{Z_aZ_Ae^2}{r_c}+U_{aA}(r_c)=E \qquad (17)$$

that allow the determination of l_c and r_c. In actual cases these quantities are not calculated from the above simple estimation but by solving explicitly the classical equations of motion as in Ref. [15].

In the presence of couplings, the energy of relative motion is not well defined, an exchange of energy from the relative motion to the intrinsic degrees of freedom takes place, and thus the above formulas for the fusion cross section have to be modified to incorporate this effect. To illustrate these modifications we will follow the work of Refs. [11,12]. Here we will only outline the main results referring to the above papers for details. To this purpose it is convenient to simplify the above Hamiltonian and consider only head-on collisions and a single surface mode in the target. The Hamiltonian becomes

$$\hat{H}=\hbar\omega a^{\dagger}a+f(t)(a^{\dagger}+a) \qquad (18)$$

with

$$f(t)=-\sqrt{\frac{\hbar\omega}{2C}}R_A\frac{\partial U_{aA}}{\partial r}. \qquad (19)$$

It is convenient to express the solution of the problem in term of the characteristic function defined by the matrix element

$$Z(\beta)=\langle\Psi(t)|e^{i\hat{H}\beta}|\Psi(t)\rangle, \qquad (20)$$

$|\Psi(t)\rangle$ being the state vector of the system. The probability to have, at time t, an energy loss E may be calculated via the Fourier transform of this function

$$P(E)=\frac{1}{2\pi}\int_{-\infty}^{+\infty}e^{-i\beta E}Z(\beta)d\beta. \qquad (21)$$

As is well known the system represented by Eq. (18) can be solved exactly; its characteristic function has the form

$$\ln Z(\beta)=|\eta(t)|^2(e^{i\hbar\omega\beta}-1)-i\frac{|f(t)|^2}{\hbar\omega}\beta \qquad (22)$$

with

$$\eta(t)=\frac{1}{i\hbar}\int_{-\infty}^{t}f(t')e^{i\omega t'}dt'+\frac{f(t)}{\hbar\omega}e^{i\omega t}. \qquad (23)$$

The function of Eq. (22) is the characteristic function of a Poisson distribution, thus the probability that the energy dissipated from the relative motion has a given value $E(t)$ is

$$P(E)=\sum_N\frac{|\eta|^{2N}}{N!}e^{-|\eta|^2}\delta\left(E+\frac{f(t)^2}{\hbar\omega}-N\hbar\omega\right), \qquad (24)$$

where N is an integer defining the number of phonons. The distribution has an average energy

$$\langle E(t)\rangle=\frac{1}{i}\frac{d}{d\beta}\ln Z(\beta)\Bigg|_{\beta=0}=\hbar\omega|\eta(t)|^2-\frac{f(t)^2}{\hbar\omega} \qquad (25)$$

and a standard deviation

$$\sigma_E^2=\frac{1}{i^2}\frac{d^2}{d\beta^2}\ln Z(\beta)\Bigg|_{\beta=0}=(\hbar\omega)^2|\eta(t)|^2. \qquad (26)$$

It is interesting to notice that the energy distribution given by Eq. (24) does not start from zero but is shifted by an amount ΔE

$$\Delta E=-\frac{f(t)^2}{\hbar\omega} \qquad (27)$$

which corresponds to the adiabatic polarization term.

The results obtained from the simple model indicate that the effect of the coupling may be taken into account by implying that the two ions move along a trajectory in the field:

$$U^N(r)=U_{aA}(r)+\langle E\rangle, \qquad (28)$$

with $\langle E\rangle$ the average energy loss given by Eq. (25). This means that at distance of closest approach the projectile meets a distribution of barriers with probabilities given by Eq. (24), the actual transmission coefficient is thus calculated by folding the transmission coefficient of Eq. (12) with the barrier distribution probability of Eq. (24). This result is very similar to the one obtained in Refs. [5,6,8,9]; for more details see Ref. [12].

The role played by the angular momentum may be easily included in this semiclassical formalism, since for the penetrability of the barrier it is important to estimate the shift and the fluctuations of the radial component of the relative motion energy. In presence of angular momentum the Hamiltonian of Eq. (18) becomes

$$\hat{H}(t)=\sum_\mu\{\hbar\omega_\lambda a_\mu^{\dagger}a_\mu+f_{\lambda\mu}(t)a^{\dagger}+f_{\lambda\mu}^*(t)a\}, \qquad (29)$$

where the sum runs over all the μ components of the angular momentum λ and the form factors are expressed in the form

$$f_{\lambda\mu}(t)=-\sqrt{\frac{\hbar\omega_\lambda}{2C_\lambda}}\frac{\partial U_{aA}(r)}{\partial r}R_AY_{\lambda\mu}^*\left(\frac{1}{2}\pi,\Phi(t)\right), \qquad (30)$$

C_λ being the restoring force parameter. Indicating with **I** and **L** the intrinsic angular momentum and the orbital angular momentum, respectively, we may write the radial energy in the form

$$E_r=\hat{H}(t)-\frac{(\mathbf{L}-\mathbf{I})^2-\mathbf{L}^2}{2m_{aA}r^2}. \qquad (31)$$

This, in good approximation, may be rewritten as

$$E_r = \hat{H}(t) - \sum_\mu \hbar\mu\dot{\Phi}(t)a_\mu^\dagger a_\mu, \qquad (32)$$

where $\dot{\Phi}(t)$ is the angular velocity. From the above expression one can immediately deduce that the effect of the angular momentum can be included by using the old results but with the substitution

$$\omega \rightarrow [\omega - \mu\dot{\Phi}(t)]. \qquad (33)$$

It is clear that the transfer of angular momentum starts to be important at energy very close or above the Coulomb barrier where it will strongly influence the shape of the barrier distribution.

In order to include the transfer channels in the barrier penetration problem we will follow Ref. [11] where a consistent description of particle transfer and dissipation of energy in heavy ion reactions has been obtained by treating the transfer channels as mutually independent and also independent on the excitation of the collective surface modes. Here we will use the result that the transfer probability is quite small and that the large dissipated energy and large mass and charge drift are due to the very large number of transfer channels. From the hypothesis of independence we can immediately conclude that the characteristic function describing the properties of these reactions may be written as

$$Z_{tr}(\beta) = \prod_\gamma Z_{tr}^\gamma(\beta); \qquad (34)$$

here the product has to be taken over all neutron stripping (νS), neutron pick-up (νP), proton stripping (πS), and proton pick-up (πP) channels. For the case of neutron stripping one gets [12]

$$\ln Z_{tr}^{\nu S}(\beta) = \sum_{i'k} \left| \frac{\tau_\nu}{2\hbar\xi_{ki'}} f^{ki'}(r_0) \right|^2 \left[|s(\xi_{ki'})|^2 \right.$$
$$\left. \times (e^{i(2\hbar\xi_{ki'}/\tau_\nu)\beta} - 1) - i\frac{2\hbar\xi_{ki'}}{\tau_\nu}\beta \right], \qquad (35)$$

where the sum has to be extended over all the single particle states of projectile (i') and target (k). This expression has been obtained by using for the single-particle transfer form factor an exponential shape $f^{ki'}(r) \simeq e^{\kappa_\nu(r-R_0)}$ where κ_ν defines the range of the form factor that is almost twice the one for inelastic processes. The function $s(\xi_{ki'})$ weights the contribution of the different transfer channels (see Ref. [12]). The collision time and the adiabaticity parameters are here defined by

$$\tau_\nu = \frac{1}{\sqrt{\kappa_\nu \ddot{r}_0}}, \qquad (36)$$

$$\xi_{ki'} = \frac{\tau_\nu}{2\hbar}[(\epsilon_{i'} - \epsilon_k) - \hbar(m_{i'} - m_k)\dot{\Phi}_0 + Q_0], \qquad (37)$$

where ϵ and m are the energy and the magnetic quantum number identifying the single-particle state. With Q_0 we have indicated the optimum Q value for the transition. For the case of neutron transfer it may be assumed to be zero while for the case of proton stripping has the expression

$$Q_0 = \frac{(Z_a - Z_A)e^2}{r_0}. \qquad (38)$$

In the above expressions with $\ddot{r}_0$ and $\dot{\Phi}_0$ we have indicated the radial acceleration and the angular velocity at the distance of closest approach r_0 for the given trajectory.

In the estimation of the barrier penetration we will not include the contribution of particle transfer channels to the average energy loss but only their contribution to the energy spread. This is because the estimation of $\langle E \rangle$, through the sum over all single particle states, is diverging and its value will strongly depend on the assumed energy cutoff for the single particle form factor to vanish. We remind that the nuclear potential of Eq. (6) has been obtained via a best-fit procedure over elastic scattering data and part of the polarization is automatically included. We observe also that this polarization term is proportional to the square of the single-particle form factors and thus has a shape that is very similar to the potential itself.

For the spread in energy we obtain

$$(\sigma_{E_r}^{\nu S})^2 = \frac{1}{i^2}\frac{d^2}{d\beta^2}\ln Z_{tr}^{\nu S}(\beta)\bigg|_{\beta=0} = \sum_{i'k} |f^{ki'}(r_0)|^2 |s(\xi_{ki'})|^2. \qquad (39)$$

In the evaluation of the above expression we replace the sum over the discrete levels of projectile and target with an integral over a continuous distribution and we replace the single
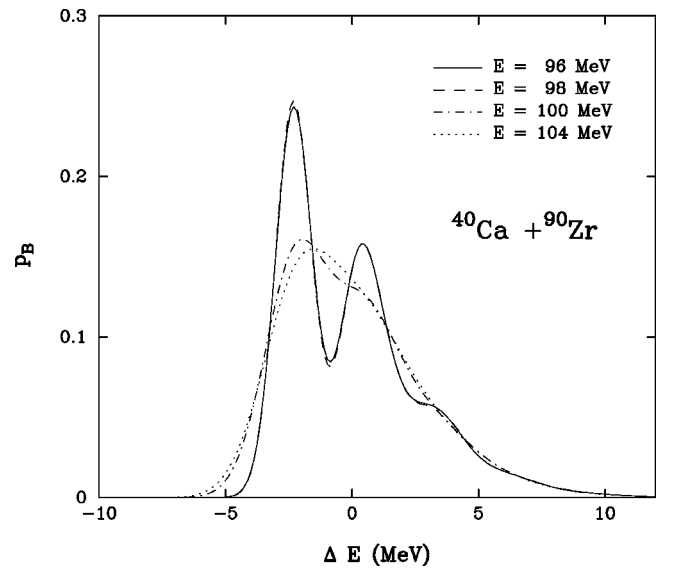

FIG. 1. Theoretical barrier distributions for the ^{40}Ca$+$^{90}Zr system for the indicated center-of-mass bombarding energies. Notice that the shape of the barrier distribution changes very little for energies below the Coulomb barrier.
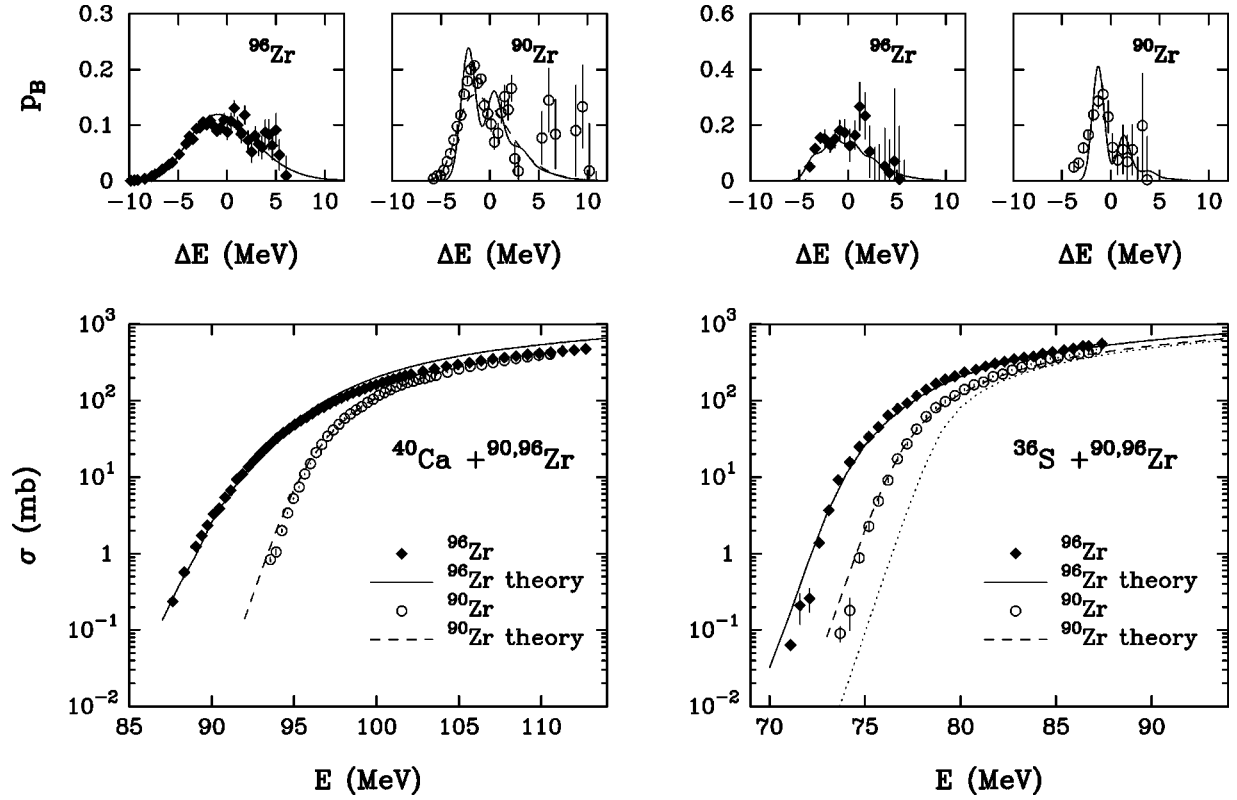
FIG. 2. In the bottom row, for the indicated systems, are shown the calculated excitation functions in comparison with the experimental data. For the case of $^{36}S + ^{90}Zr$ we show also (dotted line) the uncoupled results. In the top row the calculated barrier distributions are compared with the experimental ones. The theoretical curves have been obtained for an energy below the Coulomb barrier.

particle form factors with the average as discussed in Ref. [16]. For the single particle neutron level density we use the expression

$$g_\nu(\epsilon,m) = g_0^\nu \sqrt{\frac{1}{2\pi b_\nu} \frac{\epsilon_F - V_{A0}}{\epsilon - V_{A0}}} \exp\left[-\frac{m^2}{2b_\nu} \frac{\epsilon_F - V_{A0}}{\epsilon - V_{A0}}\right], \quad (40)$$

where with ϵ_F we have indicated the Fermi energy, with V_{A0} the depth of the shell model potential and with m the magnetic quantum number. The parameter b_ν is related to the mean values of m^2 and may be expressed as a function of the rigid moment of inertia and g_0^ν is the neutron level density at the Fermi surface. For more details see Ref. [12].

Since the different transfer modes are considered to be independent the total width of the distribution due to particle transfer is given by

$$\sigma_{tr}^2(E_r) = \sum_\gamma [\sigma_{tr}^\gamma(E_r)]^2 \quad (41)$$

where the index γ has been defined above. In conclusion the probability to have a given value E_r of energy loss in radial energy may be written in the form

$$P(E_r) = \sum_{\{N_n\}} \left(\prod_n \frac{|\eta_n|^{2N_n}}{N_n!} e^{-|\eta_n|^2}\right) G(E_r - E_{\{N_n\}}), \quad (42)$$

where G is a Gaussian distribution with standard deviation given by Eq. (41) and

$$E_{\{N_n\}} = \sum_n \left[\sum_\mu N_n(\hbar\omega_n - \mu\dot{\Phi}_0) - \frac{f_{\lambda_n}^2(r_0)}{\hbar\omega_n - \mu\dot{\Phi}_0}\right]. \quad (43)$$

In the above expressions the index n runs over all the surface modes included in the calculation and we have indicated with $\{N_n\}$ the set of integers defining the occupation numbers of the surface modes. The fusion cross section may be thus calculated from Eq. (10) where the transmission coefficient is defined by

$$T_l(E) = \int_{-\infty}^{+\infty} P(E_r)T_l(E - E_r)dE_r. \quad (44)$$

Before proceeding to the applications of the above formalism to the calculation of fusion data a last consideration about the definition in Eq. (12) of the transmission coefficient. The fact that the surfaces are not static but can vibrate will influence the penetrability of the barrier. As discussed in Ref. [12] this effect may be incorporated by modifying the mass parameter by substituting $1/m_{aA}$ with $(1+\delta)/m_{aA}$ where δ is given by Eq. (15).

TABLE I. Energy and strength of the low lying 2^+ and 3^- states included in the calculations. The values are taken from Refs. [18,19].

Nucleus	E_{2^+} (MeV)	$BE2$ ($e^2 b^2$)	E_{3^-} (MeV)	$BE3$ ($e^2 b^3$)
^{12}C	4.439	4.10×10^{-3}	9.641	6.10×10^{-4}
^{16}O	6.917	4.01×10^{-3}	6.130	1.50×10^{-3}
^{32}S	2.230	3.00×10^{-2}	5.006	1.05×10^{-2}
^{36}S	3.291	9.60×10^{-3}	4.200	7.00×10^{-3}
^{40}Ca	3.904	9.60×10^{-3}	3.737	2.04×10^{-2}
^{48}Ca	3.832	8.40×10^{-3}	4.507	8.30×10^{-3}
^{58}Ni	1.454	6.95×10^{-2}	4.475	1.70×10^{-2}
^{60}Ni	1.332	9.33×10^{-2}	4.040	2.08×10^{-2}
^{90}Zr	2.186	6.30×10^{-2}	2.750	1.08×10^{-1}
^{96}Zr	1.750	5.50×10^{-2}	1.897	1.86×10^{-1}
^{110}Pd	0.374	8.70×10^{-1}	2.038	9.80×10^{-2}
^{124}Sn	1.132	1.66×10^{-1}	2.614	7.30×10^{-2}
^{140}Ce	1.596	2.95×10^{-1}	2.470	2.10×10^{-1}
^{144}Sm	1.660	2.66×10^{-1}	1.810	2.70×10^{-1}
^{154}Sm	0.082	4.36	1.013	1.00×10^{-1}
^{194}Pt	0.328	1.66	1.433	1.31×10^{-1}
^{198}Pt	0.407	1.06		
^{208}Pb	4.085	2.90×10^{-1}	2.615	6.11×10^{-1}

III. COMPARISON WITH THE DATA

In this section we will apply the above formalism, by using the program GRAZING [17], to the calculation of fusion excitation functions for a variety of target and projectile combinations focusing on systems where together with the excitation function also the barrier distribution could be obtained. Let us remind that the fusion cross section is calculated from Eqs. (10) and (44). It is thus clear that in our model, contrary to all other approaches where the barrier distributions are inferred from the excitation functions, in order to calculated the fusion cross sections we must first calculate the barrier distributions. They are energy dependent and their shapes are determined by the dynamics of the collision and by the properties of the intrinsic degrees of freedom of the colliding nuclei. Therefore, before going into the detail of the comparison with the experimental data, we will start by discussing the properties of the barrier distributions.

For the ^{36}S + ^{90}Zr system we show in Fig. 1, for the indicated center-of-mass energies, the calculated barrier distributions as a function of the parameter ΔE that measures the uncertainty in the energy of radial motion due to the excitation of the intrinsic states (the zero of this scale corresponds to the center-of-mass energy E). At energies below the Coulomb barrier (for this system it is at $\simeq 101$ MeV) the barrier distribution maintains the same shape while at energies above it becomes smoother and wider. This behavior, as discussed in the theory section, is governed by the partial wave distribution of the fusion cross section, in fact at energies below the Coulomb barrier the average l value of the compound nucleus is essentially constant while it increases at larger energies thus contributing to smooth out the barrier distribution [see Eq. (33)]. The particle transfer degrees of

freedom play a minor role and contribute, also, to smooth-out the barrier distribution at higher energies.

In the following in comparing our barrier distributions with the experimental ones, extracted from the excitation functions, we will shift and scale the "experimental data" to superimpose on our calculated curves and we will show the barrier distribution calculated at an energy below the Coulomb barrier. The relative motion and the nuclear form factors for the excitation of the surface modes are determined, in our model, by the nuclear potential of Eq. (6) that has been determined by a best fit procedure of elastic scattering data on several target and projectile combinations. In order to have a better fit to the experimental data we introduce, in our formalism, two parameters. The first one ΔR is a shift in the nuclear potential radius [see Eq. (6)], while the second one s_δ is a scaling of the correction δ to the reduced mass that enters in the calculation of the transmission coefficient [see Eq. (15)]. We thus make the following substitutions:

$$R_a + R_A \rightarrow R_a + R_A + \Delta R \qquad (45)$$

and

$$\delta \rightarrow s_\delta \delta. \qquad (46)$$

We remember that Eq. (15) gives an estimation of δ only for the nuclear interaction, in actual cases one should also con-

TABLE II. The values of the parameters ΔR and s_δ, for the indicated reactions, used in the calculations.

| Reaction	ΔR (fm)	s_δ	Ref.
^{40}Ca + ^{90}Zr	-0.15	0.1	[29]
^{40}Ca + ^{96}Zr	-0.02	0.8	[29]
^{36}S + ^{90}Zr	0.0	0.0	[25]
^{36}S + ^{96}Zr	0.1	0.0	[25]
^{12}C + ^{194}Pt	-0.15	0.0	[20]
^{12}C + ^{198}Pt	-0.2	0.0	[20]
^{16}O + ^{144}Sm	-0.2	0.0	[21]
^{16}O + ^{154}Sm	-0.33	0.0	[21]
^{32}S + ^{110}Pd	0.0	0.6	[24]
^{36}S + ^{110}Pd	0.2	0.2	[24]
^{16}O + ^{208}Pb	-0.05	0.0	[22,23]
^{40}Ca + ^{124}Sn	0.05	0.9	[31]
^{36}S + ^{140}Ce	-0.05	0.2	[26]
^{40}Ca + ^{194}Pt	-0.2	0.5	[30]
^{40}Ca + ^{46}Ti	0.0	0.2	[28]
^{40}Ca + ^{48}Ti	-0.1	0.3	[28]
^{40}Ca + ^{50}Ti	-0.2	0.8	[28]
^{46}Ti + ^{64}Ni	0.15	0.5	[32]
^{48}Ti + ^{64}Ni	0.05	0.5	[33]
^{40}Ca + ^{40}Ca	-0.2	0.25	[27]
^{40}Ca + ^{48}Ca	-0.1	0.8	[27]
^{58}Ni + ^{58}Ni	-0.1	0.8	[34]
^{58}Ni + ^{64}Ni	0.0	0.8	[34]
^{64}Ni + ^{64}Ni	0.03	0.5	[35]
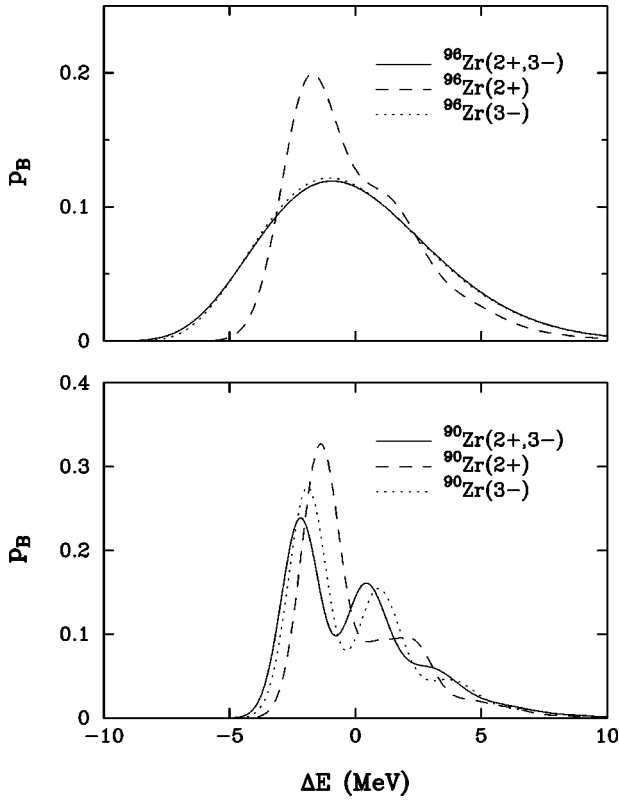
FIG. 3. Theoretical barrier distributions for the ^{40}Ca+^{90,96}Zr systems as a function of the states of the target included in the calculations. The full curve indicates the results when both the 2^+ and 3^- states have been included, the dashed one when only the 2^+ state is included and the dotted one when only the 3^- state is included in the calculation. Notice that all distributions are normalized to one.

sider the Coulomb one that has a counter effect. With these two parameters we are able to achieve a reasonable overall description of the data.

In Fig. 2 we display the calculated excitation functions (bottom) and the corresponding barrier distributions (top) for the ^{40}Ca+^{90,96}Zr and ^{36}S+^{90,96}Zr systems in comparison with the experimental data. In the calculations we have included the low-lying 2^+ and 3^- states of target and projectile as reported in Table I and the potentials have been modified according to the parameters of Table II. For the system ^{36}S+^{90}Zr we report also the uncoupled excitation function. For these reactions it is interesting to understand the remarkable difference between the excitation functions of the two Zirconium isotopes since they have quite similar spectra. In Ref. [29] this difference has been tentatively ascribed to particle transfer channels, particularly to neutron transfer. In Fig. 3 we display for the ^{40}Ca+^{90,96}Zr systems the evolution of the barrier distributions as a function of the target states included in the calculation. It is clear that the difference in the barrier distribution has to be ascribed to the strength on the 3^- state that is stronger in the case of ^{96}Zr.

In Figs. 4, 5, and 6 we show a systematic comparison of our calculations with the experimental data both for excitation functions and barrier distributions when they are available. When the same projectile or target is used for different targets or projectiles, the corresponding data are displayed in the same frame to facilitate the comparison. All the calculations have been performed by including the low-lying 2^+ and 3^- states of projectile and target and including all the transfer channels as discussed in the previous section (see Table I for the energy and strength of the inelastic states and Table II for the parameters ΔR and s_δ used). The high-lying
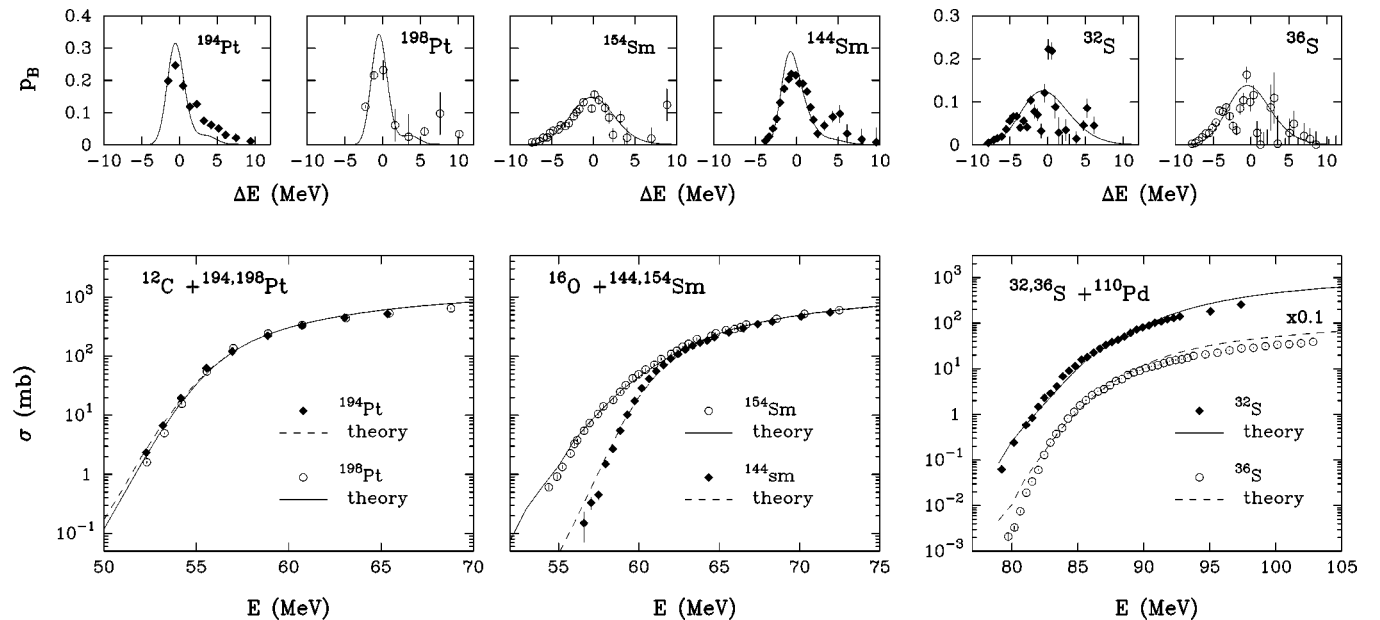

FIG. 4. Excitation functions (bottom row) and barrier distributions (top row) for the indicated systems. Notice that the excitation function for the ^{36}S+^{110}Pd system has been scaled by an order of magnitude.
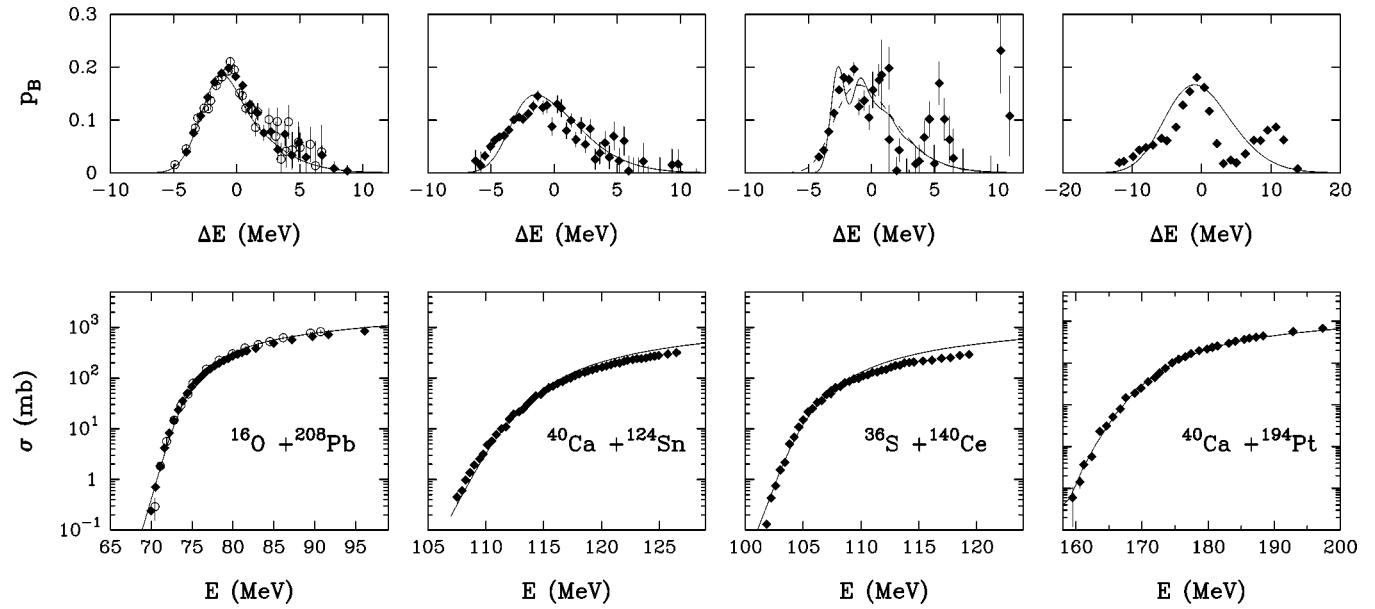
FIG. 5. Excitation functions (bottom row) and barrier distributions (top row) for the indicated systems. For the ^{32}S+ ^{140}Ce a barrier distribution calculated at an energy above the Coulomb barrier (dashed line) is also shown. For the ^{16}O+ ^{208}Pb are shown the two sets of experimental data of Refs. [22,23].

states have not been included in our calculations since their effect on the barrier distribution is negligible and they account for an overall normalization of the fusion excitation functions of a few percent. The overall agreement between data and theory is quite good especially for the cases of Figs. 4 and 5 where together with the fusion excitation functions also the corresponding barrier distributions were available. As a general remark we mention that our theory does not predict any bumps at high energy as indeed it is shown by

the data of ^{12}C+ ^{196}Pt, ^{16}O+ ^{144}Sm, ^{36}S+ ^{140}Ce, and ^{40}Ca + ^{194}Pt. For some systems, for instance ^{36}S+ ^{140}Ce, we overestimate the fusion cross section in the high-energy part but, in this region, one should keep in mind that for those systems, at high energy, the fission channel starts to play an important role and this channel can account for part of the missing fusion cross section. For the cases displayed in the last figure (Fig. 6) discrepancies are clearly seen for the nickel on nickel and calcium on calcium reactions but our
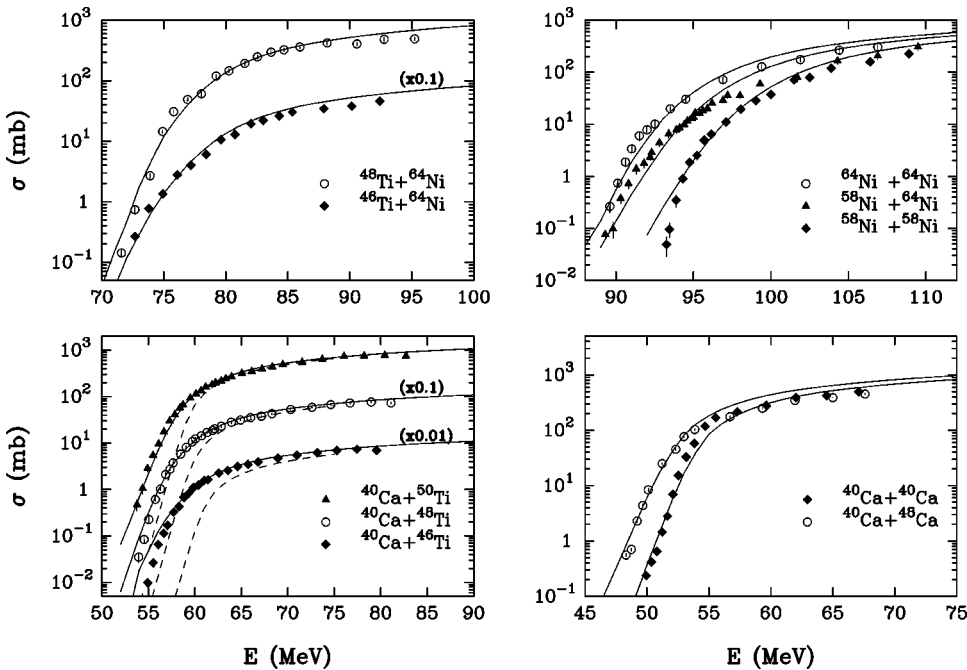

FIG. 6. Excitation functions for the indicated systems. For the ^{40}Ca+ ^{X}Ti also the uncoupled excitation functions are shown (dashed line).

curves are of the same quality as the one of previous analyses, see, for instance, Ref. [36], where the influence of higher order couplings has been investigated.

IV. CONCLUSIONS

In this paper we have used the semiclassical model of Refs. [11,12], that incorporates on the same footing transfer channels and the inelastic excitation to the low-lying states to the calculation of excitation functions and barrier distributions. The systematics over several combinations of target and projectile demonstrates that the model gives an adequate description of the processes and stresses the importance of a proper treatment of the inelastic collective degrees of freedom in order to have a correct description of the dynamical evolution of the nuclear surfaces that dominates the process in question.

---

[1] L. C. Vaz, J. M. Alexander, and G. R. Satchler, Phys. Rep. **69**, 373 (1981).

[2] M. Beckerman, Phys. Rep. **129**, 145 (1985).

[3] H. Esbensen, Nucl. Phys. **A352**, 147 (1981).

[4] H. Rowley, G. R. Satchler, and P. H. Stelson, Phys. Lett. B **254**, 25 (1991).

[5] C. H. Dasso, S. Landowne, and A. Winther, Nucl. Phys. **A405**, 381 (1983).

[6] C. H. Dasso, S. Landowne, and A. Winther, Nucl. Phys. **A407**, 221 (1983).

[7] C. H. Dasso, S. Landowne, and A. Winther, Nucl. Phys. **A432**, 495 (1985).

[8] C. H. Dasso and S. Landowne, Comput. Phys. Commun. **46**, 187 (1987).

[9] J. O. Fernandez-Niello, C. H. Dasso, and S. Landowne, Comput. Phys. Commun. **54**, 409 (1989).

[10] K. Hagino, N. Rowley, and A. T. Kruppa, Comput. Phys. Commun. **123**, 143 (1999).

[11] A. Winther, Nucl. Phys. **A572**, 191 (1994).

[12] A. Winther, Nucl. Phys. **A594**, 203 (1995).

[13] R. Broglia and A. Winther, *Heavy Ion Reactions* (Addison-Wesley, Redwood City, CA, 1991).

[14] R. A. Broglia, C. H. Dasso, and A. Winther, in *Proceedings of Enrico Fermi International School of Physics*, 1979, edited by R. A. Broglia, C. H. Dasso, and R. Ricci (North-Holland, Amsterdam, 1981).

[15] C. H. Dasso and G. Pollarolo, Comput. Phys. Commun. **50**, 341 (1988).

[16] J. M. Quesada, G. Pollarolo, R. A. Broglia, and A. Winther, Nucl. Phys. **A442**, 381 (1985).

[17] A. Winther, GRAZING, computer program (unpublished).

[18] S. Raman, C. W. Nestor, Jr., S. Kahane, and K. H. Bhatt, At. Data Nucl. Data Tables **42**, 1 (1989).

[19] R. H. Spear, At. Data Nucl. Data Tables **42**, 55 (1989).

[20] A. Shrivastava, Ph.D. thesis, Mumbai University, Mumbai, India, 1999; in *Proceedings of the 9th International Conference on Nuclear Reaction Mechanisms*, Varenna, Italy, 2000, edited by E. Gadioli (Ricerca Scientifica ed Educazione Permanete, Milano, 2000).

[21] J. R. Leigh, M. Dasgupta, D. J. Hinde, J. C. Mein, C. R. Morton, R. C. Lemmon, J. P. Lestone, J. O. Newton, H. Timmers, and J. X. Wei, Phys. Rev. C **52**, 3151 (1995).

[22] C. R. Morton, D. J. Hinde, J. R. Leigh, J. P. Lestone, M. Dasgupta, J. C. Mein, J. O. Newton, and H. Timmers, Phys. Rev. C **52**, 243 (1995).

[23] C. R. Morton, A. C. Berriman, M. Dasgupta, D. J. Hinde, J. O. Newton, K. Hagino, and I. J. Thompson, Phys. Rev. C **60**, 044608 (1999).

[24] A. M. Stefanini, D. Ackermann, L. Corradi, J. H. He, G. Montagnoli, S. Beghini, F. Scharlassara, and G. Segato, Phys. Rev. C **52**, R1727 (1995).

[25] A. M. Stefanini, L. Corradi, A. M. Vinodkumar, Yang Feng, F. Scarlassara, G. Montagnoli, S. Beghini, and M. Bisogno, Phys. Rev. C **62**, 014601 (2000).

[26] A. Stefanini (private communication).

[27] H. Aljuwair, R. J. Ledoux, M. Beckerman, S. Gazes, J. Wiggins, E. R. Cosman, R. R. Betts, S. Saini, and Ole Hansen, Phys. Rev. C **30**, 1223 (1984).

[28] A. A. Sonzogni, J. D. Bierman, M. P. Kelly, L. P. Lestone, J. F. Liang, and R. Vandenbosch, Phys. Rev. C **57**, 722 (1998).

[29] H. Timmers, D. Ackermann, S. Beghini, L. Corradi, J. H. He, G. Montagnoli, F. Scarlassara, A. M. Stefanini, and N. Rowley, Nucl. Phys. **A633**, 421 (1998).

[30] J. D. Bierman, P. Chan, J. F. Liang, M. P. Kelly, A. A. Sonzogni, and R. Vandenboch, Phys. Rev. Lett. **76**, 1587 (1996).

[31] F. Scarlassara, S. Beghini, G. Montagnoli, G. F. Segato, D. Ackermann, L. Corradi, C. J. Lin1, A. M. Stefanini, and L. F. Zheng, Nucl. Phys. **A672**, 99 (2000).

[32] N. V. S. V. Prasad, A. M. Vinodkumar, A. K. Sinha, K. M. Varier, D. L. Sastry, N. Madhavan, P. Sugathan, D. O. Kataria, and J. J. Das, Nucl. Phys. **A603**, 176 (1996).

[33] A. M. Vinodkumar, K. M. Varier, N. V. S. V. Prasad, D. L. Sastry, A. K. Sinha, N. Madhavan, P. Sugathan, D. O. Kataria, and J. J. Das, Phys. Rev. C **53**, 803 (1996).

[34] M. Beckerman, J. Ball, H. A. Henge, M. Salomaa, A. Sperduto, S. Gazes, A. DiRienzo, and J. D. Molitoris, Phys. Rev. C **23**, 1581 (1981).

[35] M. Beckerman, M. Salomaa, A. Sperduto, J. D. Molitoris, and A. DiRienzo, Phys. Rev. C **25**, 837 (1982).

[36] H. Esbensen and S. Landowne, Phys. Rev. C **35**, 2090 (1987).